Chapter 7

SERS-Based Sensitive Detection of Organophosphorus Nerve Agents

Qian Zhao, Guangqiang Liu and Weiping Cai

Additional information is available at the end of the chapter

http://dx.doi.org/10.5772/intechopen.72630

Abstract

Organophosphorus nerve agents, such as sarin, tabun, cyclosarin and soman, belong to the most toxic substances. So, it is very important to quickly detect it in trace-level and on-site or portable way. But, both fast and trace detections have been expected because current techniques are of low sensitivity or of poor selectivity and are time-consuming. The surface-enhanced Raman scattering (SERS)-based detection could be a suitable and effective method. However, the organophosphorus nerve agents only very weakly interact with highly SERS-activated noble metal substrates and are hardly adsorbed on them. In this case, it is difficult to detect such molecules, with reproducible or quantitative measurements and trace level, by the normal SERS technique. Recently, there have been some works on the SERS-based detection of the organophosphorus molecules. In this chapter, we introduce the main progresses in this field, including (1) the thin water film confinement and evaporation concentrating strategy and (2) the surface modification and amidation reaction. These works provide new ways for highly efficient SERS-based detection of the organophosphorus nerve agents and some other target molecules that weakly interact with the coin metal substrates.

Keywords: SERS-based sensitive detection, organophosphorus nerve agents, thin water film confinement, concentrating-enhanced Raman scattering effect, surface modification, amidation reaction

1. Introduction

Organophosphorus nerve agents (such as sarin, tabun, cyclosarin and soman, etc.) belong to the high-risk chemicals with strong poison [1]. When a person is exposed to such nerve agents, sarin for example, with 1.43 ppm, death would occur in few minutes if the agent is inhaled through his/her respiratory system. Even if the nerve agent enters the body through the skin or

through consumption, poisoning would occur in few hours [2]. It is thus vital to fast detect them in highly sensitive and portable way. There have existed some methods for the detection of these organophosphorus molecules, such as gas chromatography coupled to a mass spectrometer, ion mobility time-of-flight mass spectrometry, gas sensing and microcantilever, and so on [2–5]. But, these current techniques are of low sensitivity or of poor selectivity and are time-consuming. Both quick and trace detection of them have been expected and are most challenging.

The detection based on surface-enhanced Raman scattering (SERS) effect, which has been extensively reported since its discovery in the 1970s [6–14], would be an appropriate and effective method for fast and ultrasensitive detection. The SERS effect originates from a significant enhancement in the effective Raman cross-section of the target molecules situated at or very near to the roughened noble metal surfaces or colloidal particles [15–25]. The detection based on the SERS effect has the characteristics of high sensitivity, fast response and fingerprint recognition with the ability to be close to a single molecule level [26–29]. The main contribution of amplification of Raman signal intensity arises from the local electromagnetic field enhancement due to the surface plasmon resonance (SPR) of the metal nanoparticles, which has been extensively reported [15–21]. In a conventional SERS detection technique, the target molecules need to stay on the "hot spots" or within the strong electromagnetic field enhancement areas above the SERS substrates [30, 31]. Traditionally, the SERS-based detection is limited to the target molecules, which have high affinity with the metal (gold or silver, etc.) surfaces. It is thus a prerequisite that the substrates can capture or adsorb the target molecules within the strong field-enhancement areas or on the hot spots for the SERS-based detection. However, the organophosphorus nerve agents (including sarin, cyclosarin and soman, etc.) have only very weak interaction (or even no affinity) with highly SERS-activated noble metal substrates and are hardly adsorbed on the substrates or have only very short residence time on them. Obviously, in this case, the normal SERS-based technique is difficult to realize the effective detection of such molecules [13, 32]. For instance, the organophosphorus molecule dimethyl methylphosphonate (DMMP, a typical sarin simulant agent), which is hardly adsorbed on the noble metal surfaces [33], is very difficult to be detected by the SERS-based technique with reproducible measurements and trace level [33, 34]. This is the reason why there have only been very limited reports on the SERS-based detection of the organophosphorus molecules that could only weakly interact with the noble metals [35, 36].

The SERS substrates after surface modification could selectively adsorb and enrich such molecules on their surfaces. However, it is generally difficult to obtain proper modifying agents for the given target molecules and to realize the reproducible measurements and quantitative detection of them without interfering effect. Besides, for the organic modifying agents, they may induce the complicacy of Raman spectral pattern and hence misidentification. Recently, there have been some new approaches developed for the SERS-based detection of the organophosphorus molecules. In this chapter, we introduce the progresses in this field, mainly including (1) the thin water film confinement and evaporation concentrating strategy and (2) the surface modification of the SERS substrates and amidation reaction. These works have provided new ways for highly efficient SERS-based detection of the organophosphorus nerve agents and some other target molecules that weakly interact with the coin metal substrates.

2. Thin water film confinement and evaporation concentrating strategy

For the SERS-based detection of the organophosphorus nerve agents that can only weakly interact with the coin metal substrates, a new and effective route has been developed to capture the hydrosoluble organophosphorus molecules based on the thin water film confinement and evaporation concentrating strategy [33]. DMMP, which is very difficult to be captured by the noble metal substrates, was used as the target molecule, and the gold micro-/nanostructured array was employed as the SERS substrate to demonstrate the validity of this strategy. It has been confirmed that by such strategy, the noble metal SERS substrate can effectively capture the DMMP molecules, realizing SERS-based trace detection of them.

2.1. Strategy and model

2.1.1. Strategy

Normally, in the conventional detections based on the SERS effect, the SERS substrates are firstly soaked in the solution containing target molecules for a certain duration to make the molecules adsorbed on the substrate's surfaces, and then taken out and dried before spectral measurement. If the target molecules can only weakly interact with the substrates, however, such procedures would be of no avail because of no or too less molecules on the substrate's surface after drying. Here, a water film confinement and evaporation concentrating strategy could overcome the abovementioned problem, as schematically illustrated in **Figure 1**.

First, the aqueous solution containing target molecules is dropped onto a SERS-active substrate with hydrophilic surface (**Figure 1a**), which will then spread out and form a water film on the surface. The target molecules (or the solute molecules) are accordingly confined within the thin water film (see **Figure 1b**). The subsequent solvent (water) evaporation induces the thinner and thinner water film, and continuous concentrating of the solutes within the film, assuming that solute volatilization is insignificant or negligible compared with the water evaporation (see **Figure 1c**). When the water film decreases in thickness down to the nanometer level, all the target molecules confined in the water film are localized within the region above the substrate, within which the electromagnetic field can be enormously enhanced under external excitation (see **Figure 1d**). If Raman spectra are measured for this film at this moment, the Raman signal of the target molecules should be enhanced by both the concentrated solutes and the substrate surface. After complete drying, no target molecules will be left on the substrate due to their weak interaction with the substrate and hence we cannot obtain their Raman signals.

2.1.2. Concentrating factor

For quantitative analysis, the evaporation-induced concentrating factor (***CF***) of the target molecules in the water film is defined as the ratio of solute concentration (C_m) in the water film at the moment of Raman spectral measurement to that at the initial stage (C_0), or

$$CF = \frac{C_m}{C_0} \tag{1}$$

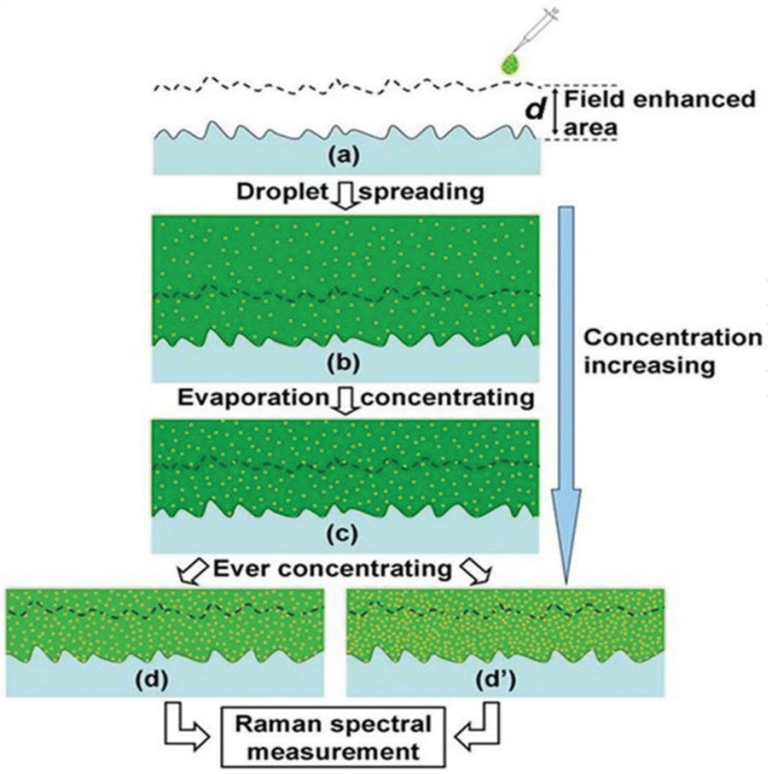

Figure 1. The schematic illustration for the water film confinement and evaporation-concentrating process. (a) A clean SERS substrate. (b) A liquid film formed on the substrate after dropping a certain amount of the solution on it. (c) The liquid film is decreased in thickness and solute is concentrated due to solvent's evaporation. (d) and (d') The liquid film is comparable in thickness to the field-enhanced space for the substrates with hydrophilic and hydrophobic surfaces, respectively [33].

Based on the above described strategy (or in **Figure 1**), if the substrate surface is hydrophilic, the concentrating factor can be approximately written as

$$CF = (1 - S) \cdot \frac{H_0}{H_m} \tag{2}$$

in which

$$S = \frac{M_0 - M_m}{M_0} \quad \text{and} \quad H_m \geq d \tag{3}$$

where $\boldsymbol{H_0}$ is the initial thickness of water film after the water droplet is spreading out on the substrate, $\boldsymbol{H_m}$ is the corresponding value when the Raman spectral measurement is performed, $\boldsymbol{d}$ is the distance (in nanometer scale) from the substrate surface and within which the electromagnetic field can be significantly enhanced during laser excitation, S is the loss-ratio of the target molecules in the water film due to the possible volatilization during solvent evaporation and $\boldsymbol{M_0}$ and $\boldsymbol{M_m}$ are the mole numbers of the target molecules in the water film at the initial and the spectral measurement stages, respectively.

Generally, compared with the evaporation of the solvent, volatilization of the molecules like DMMP in solutions is significantly slower due to the much heavier molecular weight than

water and could be ignorable. For better understanding, here, let us semiquantitatively evaluate the ***CF*** value. If letting $S \approx 0$ and $H_0 = 1$ mm, we can obtain $CF = 10^5$ when $H_m = 10$ nm, from Eq. (2). Such values should be credible in the order of magnitude. So, the solvent evaporation-induced concentrating effect is quite significant.

In addition, if the water film is on the SERS substrate with hydrophobic surface and reduced to an enough thin thickness due to the evaporation, it could horizontally shrink and decrease the coverage area on the substrate, which would induce further concentrating. Therefore, the *CF* value would be higher in the local water films than that for the substrate with hydrophilic surface, as shown in **Figure 1(d)′**. In other words, the substrate with hydrophobic surface should be of better concentrating effect.

Furthermore, according to Eq. (2), the strategy shown in **Figure 1** should be more effective for the target molecules with lower volatility and/or when the target molecule concentration in the initial aqueous solution is very low due to the evaporation-induced concentrating effect.

2.1.3. Effects of the thin water film

In this strategy, the thin water film would function as follows: (1) Limitation of the target molecules to the small region above the SERS substrates. When the water film is becoming very thin in thickness, the molecules are localized in the field-enhanced space although they are not adsorbed on the substrate's surface; (2) Enrichment of the target molecules. Solvent's evaporation will induce the concentrating or enrichment of the target molecules in the water film and the increase of the target molecules' number in the field-enhanced space above the substrate; (3) Decrease of laser-induced thermal effect. The water film can protect the target molecules from laser-induced damage. So, the Raman intensities can also be enhanced by increasing the laser excitation power and (4) The evaporation-induced reorientation of the target molecules. During solvent evaporation, the target molecules could re-orientate [37]. This would generate a significant Raman signal enhancement due to the charge-coupling between the molecules and the metallic surface.

2.2. Application in SERS-based detection of DMMP

Here, the gold hierarchically micro-/nanostructured bowl-like array was chosen as the SERS substrate and the DMMP as the target molecules to demonstrate the validity of the above thin water film confinement and evaporation concentrating strategy.

2.2.1. Surface morphology and wettability of the SERS active substrate

The fabrication process of the SERS substrate was prepared by the electrodeposition on a preformed monolayer polystyrene (PS) colloidal crystal (2 μm in PS sphere-diameter) in the $HAuCl_4$ aqueous solution at room temperature, as previously described. [38]. **Figure 2(a)** shows the typical morphology. The SERS substrate is the gold array consisting of the hexagonally arranged bowl-like pores with 2 μm in period. The skeleton among the pores in the array is built of nearly vertical quasi rod-shaped nanoparticles. The static contact angle of such substrate surface is about 105°, exhibiting the slightly hydrophobic surface (see **Figure 2b**).

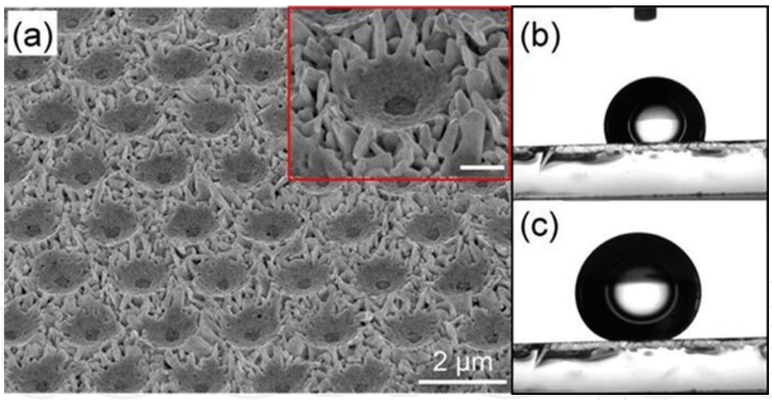

Figure 2. The morphology and wettability of a gold micro-/nanostructured array. (a) The scanning electron microscopic (SEM) image. The inset: A local magnified image and the scale bar = 500 nm. (b) and (c) The photos of the water droplets on the Au array before and after surface modification with thiol, respectively. The water droplets are 2 and 5 μL in volume for (b) and (c), respectively [33].

2.2.2. Raman spectral measurements

The DMMP aqueous solutions with different concentrations were firstly prepared and stored in a refrigerator before use. A droplet of the DMMP aqueous solution was then dropped on the SERS substrate or the gold array and spread out to form the thin water film. After evaporation at room temperature for different time intervals, the Raman spectra for the thin water film were measured on a confocal microprobe Raman spectrometer (Renishaw inVia Reflex) with a laser beam of 632.8 nm in wavelength. The Raman spectral integral time is 10 s.

Raman spectral peaks and identification. When a droplet of aqueous solution, with 20 μL in volume and 10^{-2} M DMMP in initial content, was dropped on the Au bowl-like array without surface modification, it spread out and formed a water film with about 3 mm in thickness. During the initial evaporation, no distinct Raman signal was detected for such water film on the substrate, except the background [see curve (I) in **Figure 3(a)**]. After evaporation for sufficiently long time (but without completely drying), however, a significant Raman spectrum could be observed. Typically, curve (II) in **Figure 3** shows the result corresponding to the evaporation for ~300 s after starting timing at which the distinct signals are very weak but detectable, in this experimental condition (see next subsection). At this moment, the water film was enough thin in thickness. There are one dominant Raman peak at 2936 cm^{-1} and the other three smaller peaks at 2861, 2966 and 3006 cm^{-1}, respectively. For reference, the Raman spectrum of the pure DMMP (liquid state in a quartz cell) was shown in curve (IV) of **Figure 3**, which is in good agreement with the previous report [34]. By comparison between curves (II) and (IV), there are about five wavenumbers lower for the water film than the pure DMMP. These four peaks are assigned to the C—H stretching modes of DMMP molecules [39]. Taking into consideration of the possible influence of water on the DMMP, which leads to a slight peak shift, the peaks in curve (II) of **Figure 3** can thus be attributed to the DMMP in the water film. It is well known that DMMP molecule is weak Raman scatterer with a very small cross-section on the order of 1×10–30 cm^2 under 514.5 nm excitation for the strongest line [40]. Since it is difficult to adsorb on the SERS active metal substrates, the characteristic vibration

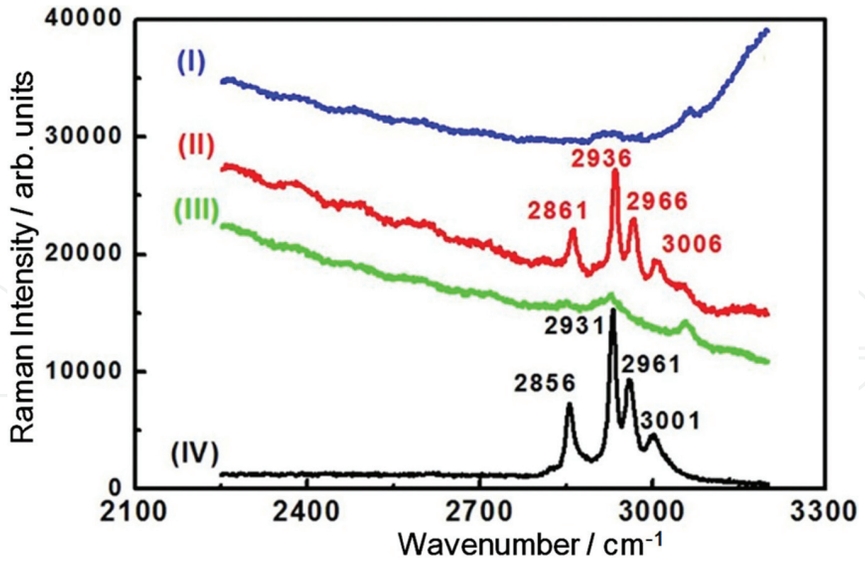

Figure 3. The Raman spectra of DMMP molecules. Curves (I), (II) and (III) are for a droplet of 10^{-2} M DMMP aqueous solution on the SERS substrate after evaporation for a very short time, a certain time and sufficiently long time (completely dried), respectively. Curve (IV): The Raman spectrum of the pure DMMP liquid. [33].

peaks of DMMP molecules in the aqueous solution are usually difficult to be detected by the SERS effect. No characteristic Raman peak from DMMP was observed after the water film was completely evaporated (see curve (III) in **Figure 3**). Obviously, such method is quite valid to detect them.

Spectral evolution with the evaporation. Further, the Raman spectral evolution of the DMMP-contained water film on the substrate with the evaporation time was measured. **Figure 4(a)** shows the spectra after evaporation for different durations for the water film with 10^{-2} M DMMP in initial concentration. During initial stage of the evaporation, no characteristic Raman signals were detected and the film is opaque in the field of optical microscope, as shown in **Figure 4(b)**. With the evaporation, the water film gets thinner and thinner. When evaporation is for t_0, which varies from several minutes to few 10 min, depending on the ambient conditions (temperature and relative humidity), the water film on the substrate was slightly transparent, and the characteristic peaks at 2936 and 2966 cm^{-1} are very weak but detectable (see curve 1) in **Figure 4(a)**. Timing begins at this moment. The further evaporation leads to appearance of the other two characteristic peaks (at 2861 and 3006 cm^{-1}) and continual enhancement of the four Raman peaks [see curves 2–6 in **Figure 4(a)**]. When the evaporation duration was up to 300 s after timing, the intensity of the characteristic Raman peaks were enhanced to the maximum, as illustrated in curve 7 in **Figure 4(a)**. The corresponding photo of the water film is given in **Figure 4 (c)**, showing translucency or semitransparence. The gold pattern on the substrate looms up. However, the longer the evaporation induced, the rapid is the decrease of the Raman signals and vanishing within ~20 s, corresponding to complete evaporation or drying. At this moment, the gold array on the substrate is clearly seen [**Figure 4(d)**]. Representatively, **Figure 5(a)** shows intensity of the dominant peak at 2936 cm^{-1} as a function of evaporation time [the data from **Figure 4(a)**] and clearly shows such evolution of the peak intensity.

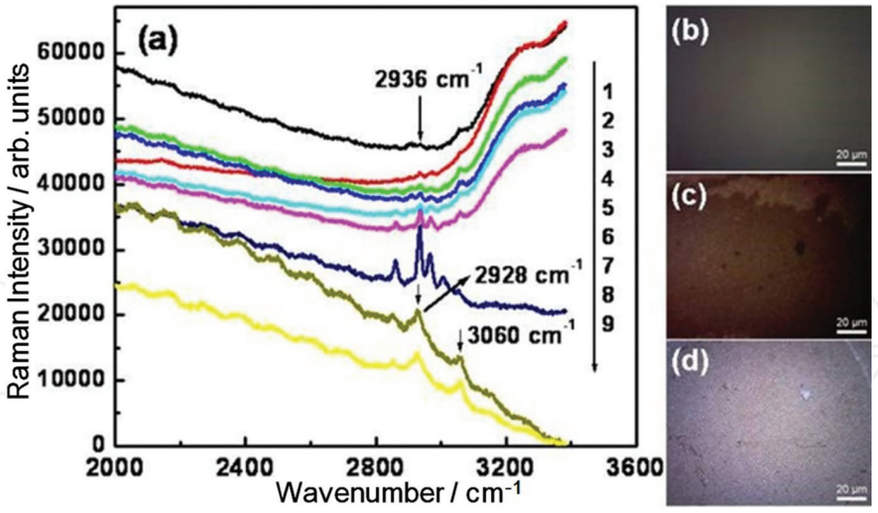

Figure 4. Raman spectra and photos of the gold array with a droplet of 10^{-2} M DMMP aqueous solution during evaporation. (a) The spectra after evaporation for different intervals. Curves 1–9 correspond to the interval Δt = 0, 112, 155, 199, 243, 279, 301, 323 and 348 s, respectively. (b)–(d) The photos of the gold array covered with water film in the initial stage, microsized-thickness and completely dried stage, respectively [33].

2.3. Concentrating-enhanced Raman scattering (CERS) effect

2.3.1. A quantitative description

The above successful observations of Raman characteristic peaks for the DMMP molecules in an aqueous solution are easily understood. This is mainly attributed to the thin water film confinement and subsequent evaporation-induced DMMP concentrating or enrichment, in addition to the electromagnetic enhancement mechanism from the Au bowl-like array. Because of the space confinement of the thin film, water evaporation induces the concentrating of DMMP within the thinner and thinner film. That is to say, more and more DMMP molecules in the water film are confined within the region with significant local electromagnetic field enhancement above the substrate, exhibiting ever-increasing Raman signal with the increasing evaporation duration, which we could call the concentrating-enhanced Raman scattering (CERS) effect, as demonstrated in **Figure 5(a)**. Obviously, after the water film is completely evaporated, the confinement effect thus vanishes. At this moment, the DMMP molecules cannot stay on the substrate due to the weak interaction, and the corresponding Raman peaks disappear. Besides, the evaporation-induced reorientation of the DMMP molecules could also induce an additional enhancement of the Raman signal owing to the charge-coupling between the molecules and the metallic surface [37].

According to the evolution of the Raman intensity with the evaporation duration shown in **Figure 5(a)**, we could semiquantitatively describe the concentrating kinetics of DMMP molecules in the water film during evaporation. First, under a given ambient condition (temperature and humidity) and a certain volume of solution droplet on the substrate with hydrophilic surface, we have the water film thickness (H) as a function of the water evaporation duration $\boldsymbol{t}$:

$$H = H_0 - V \cdot t \quad (t < t_S) \tag{4}$$

in which

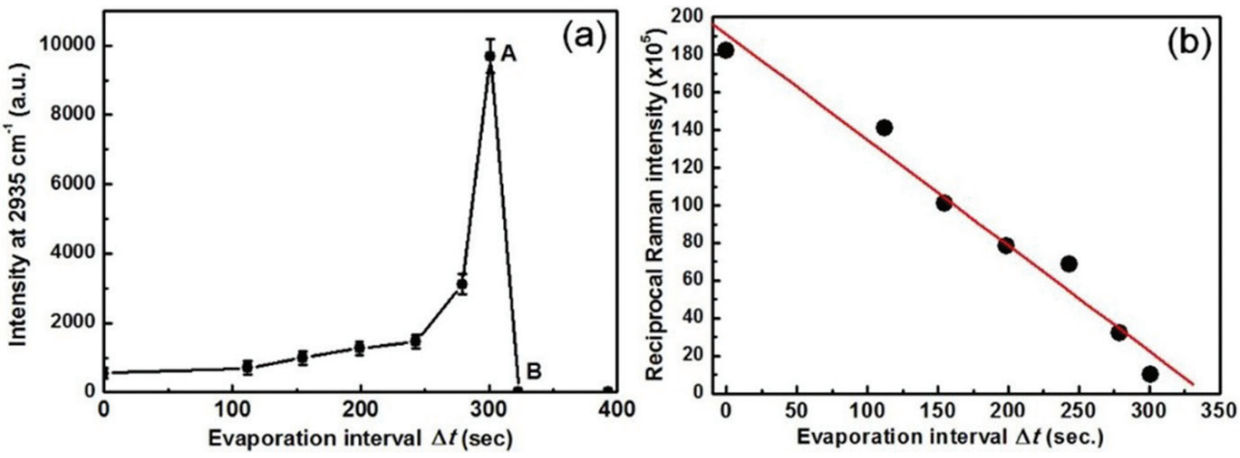

Figure 5. (a) Intensity of the Raman peak at 2936 cm^{-1} versus evaporation duration [data from **Figure 4(a)**]. Point A: The maximal measured value. Point B: The peak vanishes. (b) Plot of the reciprocal Raman intensity versus evaporation duration [data from (a)]. The solid line is the linear fitting result [33].

$$t_S = \frac{H_0}{V} \tag{5}$$

where $\boldsymbol{V}$ is the water evaporation speed (m·s^{-1} in dimension) and should be a constant independent of t, and $\boldsymbol{t_s}$ is the duration from the initial to complete evaporation.

During evaporation of solvent (water), volatilization of the solute or DMMP in water film inevitably takes place. Here, it can be assumed that its volatile rate is directly proportional to its concentration $\boldsymbol{C}$ in the water film, or

$$F = p \cdot C \tag{6}$$

where the volatile rate $\boldsymbol{F}$ is defined as the mole number volatilized in unit time and area (mol s^{-1} m^{-2}) and the parameter $\boldsymbol{p}$ is the proportional constant. So, after evaporation for $\boldsymbol{t}$, from Eq. (6), the volatile-loss ΔM of the solute (DMMP) in the film can be described by

$$\Delta M = A \cdot p \int_0^t C \cdot dt \tag{7}$$

where $\boldsymbol{A}$ is the surface area of the water film. Finally, from Eq. (7), we can quantitatively establish the relation between the solute concentration and evaporation duration of the water film, or

$$C = \frac{C_0 \cdot A \cdot H_0 - \Delta M}{A \cdot H} = \frac{C_0 \cdot H_0 - p \int_0^t C \cdot dt}{H_0 - V \cdot t} \tag{8}$$

Obviously, if $\boldsymbol{p} << 1$ or the solute is nearly involatile in the water, and/or the evaporation speed V value is relatively large enough, the volatile loss $\Delta M \approx 0$. In this case, Eq. (8) can be approximately written as

$$C \approx \frac{C_0 \cdot H_0}{H_0 - V \cdot t} \tag{9}$$

or

$$\frac{1}{C} \approx \frac{1}{C_0} - \frac{V}{C_0 H_0} \cdot (t_0 + \Delta t) \quad t = t_0 + \Delta t \tag{10}$$

where Δt is the evaporation interval after starting timing at $\boldsymbol{t_0}$ (as mentioned earlier). It means that the reciprocal solute concentration in the water film is nearly directly proportional to the evaporation duration of water. Eqs. (8) and (9) clearly indicate concentrating of the solute during evaporation.

When the solute concentration ($\boldsymbol{C}$) in the water film is low enough, intensity ($\boldsymbol{I}$) of its Raman-shift peaks should be directly proportional to $\boldsymbol{C}$. Here, DMMP is of good water solubility and much heavier molecular weight (124.08) than water [41]. Therefore, Eq. (9) could be a good description of the solute concentration evolution during water evaporation. In other words, from Eq. (10), the reciprocal intensity of the characteristic Raman peaks should be of nearly linear relation with the evaporation duration ($\boldsymbol{t}$ or Δt) of water, which has been confirmed by further spectral analysis. **Figure 5(b)** shows the results corresponding to the reciprocal Raman intensity of the peak at 2936 cm^{-1} versus the evaporation interval Δt [data from **Figure 5(a)**], showing a good linear relation between them and significant CERS effect. This also implies that the volatile loss of DMMP in water was very small or negligible during water film evaporation at ambient environment. By linear fitting, the plot in **Figure 5(b)** can be described as

$$\frac{1}{I} = 190.88 - 0.5608 \cdot \Delta t \tag{11}$$

in which the intensity $\boldsymbol{I}$ was multiplied by 10^{-5} and Δt is in second.

2.3.2. Factors influencing CERS effect

The CERS effect mentioned earlier would be influenced by some factors such as SERS active substrates, evaporation conditions and volatility of the solute, and so on. Obviously, the highly SERS active substrates, low solute's volatility and appropriate solvent's evaporation rate would be beneficial to exhibiting significant CERS effect. In addition, further experiments have revealed that the surface wettability of SERS substrate and the laser excitation power are also important to induce the strong CERS effect.

Wettability of SERS substrates surface. As mentioned in Section 2.1.2, the substrate with hydrophobic surface should be of stronger concentrating effect than that with hydrophilic surface. For confirmation, the Au micro-/nanostructured bowl-like array shown in **Figure 2(a)** was surface-modified with thiol. Correspondingly, the static contact angle was increased up to about 160° [**Figure 2(c)**], exhibiting superhydrophobic surface. Using such modified array as SERS substrate, the CERS effect was really significantly enhanced. Typically, **Figure 6** shows the Raman spectrum of DMMP on the gold array with and without surface modification,

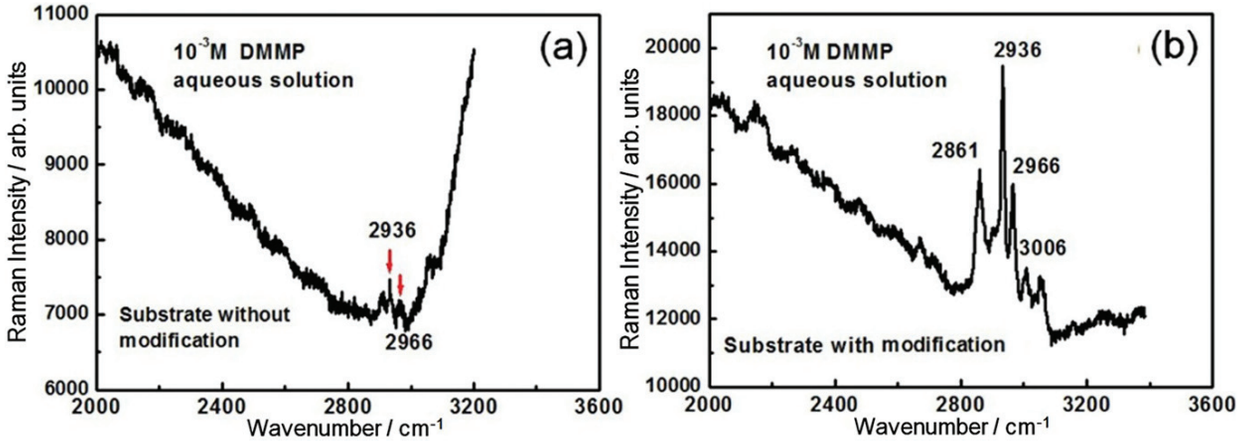

Figure 6. Raman spectra of 10^{-3} M DMMP aqueous solution on the substrates without (a) and with (b) surface modification after an optimal evaporation (the details are given in the text) [33].

measured after evaporation for an optimal duration, for the water film with 10^{-3} M DMMP in initial concentration. For the substrate without modification, the characteristic peaks of DMMP are very weak [**Figure 6(a)**]. However, the surface modification induced much stronger Raman-shift peaks of DMMP [**Figure 6(b)**], and the intensity of the dominant peak at 2936 cm^{-1} was one order of magnitude (∼12 times) higher than that without modification. Such Raman enhancement should be mainly attributed to the superhydrophobic surface-induced much higher *CF* value, which led to stronger CERS effect.

Evaporation conditions. As mentioned in Section 2.1.1, only when the thickness of the water film is reduced to the nanoscale by evaporation, the concentrating effect, that is, the CERS effect can reach the maximum. However, for the measurements in the normal ambient conditions, as shown in **Figure 4**, the thickness of the water film, corresponding to the maximal measured Raman signals could be estimated to be in micron scale (∼ 8–30 μm) according to its initial thickness and the whole time for evaporating the water droplet on the substrate. In the normal ambient conditions, it is too late to measure the Raman spectra when the water film was reduced to the nanoscale in thickness, because such thin water film would be completely evaporated or dried within one millisecond. This is the reason why the Raman peaks disappear immediately after the maximal measured value, as demonstrated in **Figure 5(a)** (points A and B). It means that the maximal measured value could be much lower than the real maximal one. Although we can obtain the *CF* value about 10^3 in order of magnitude when the water film was reduced to micron scale in thickness according to Eq. (2) and enough strong CERS effect, the real maximal or optimal effect is far from reached in the normal ambience.

Obviously, to further increase the CERS effect, we should decrease evaporation speed of the water film, especially, since $t = t_0$ at which the Raman shift peaks are weak but detectable (if the solute volatilization is neglectable). In fact, control of the evaporation speed is easily achieved. For example, we can control the evaporation rate by putting the substrate with water film into a quartz cell with a controllable opening.

Laser excitation power. Generally, the Raman scattering intensity is directly proportional to the excited laser power. But too high laser power would break down the molecules due to the

thermal effect, leading to the low Raman signal instead. However, the case here is an exception. The thin water film could protect the target molecules from the laser-induced damage because the water film can remarkably reduce the laser-induced thermal effect, as demonstrated in **Figure 7(a)**, corresponding to the Raman spectra of DMMP in the water film on the substrate, excited with different laser powers under the same evaporation duration. We could use the maximal power (P_{max} = 17 mW) of the equipment in this case, while in the conventional measurement only 5 mW or less is usually used. It has been shown that the intensity of the peak at 2936 cm^{-1} has a good linear relation with the power in whole power range, as indicated in **Figure 7(b)**. The straight line passes through the origin. So, for this thin water film confinement and evaporation concentrating strategy, one can use enough high laser excitation power (>17 mW) to further increase Raman scattering intensity, exhibiting the stronger CERS effect.

2.4. Suitability of the strategy

Based on the abovementioned text, using the thin water film confinement and evaporation concentrating strategy, one can effectively capture the hydrosoluble and weak affinity molecules within the strong electromagnetic field enhanced space above the SERS substrate and realize the SERS-based detection of them. The thin water film not only confines the target molecules within a limited space but also protects the target molecules from laser-induced damage.

It should be mentioned that the hydrophobic substrate surface, slower evaporation and stronger excitation power can further increase CERS effect. Especially, the slow and controlled evaporation in the anaphase would lead to several orders of magnitude in higher CERS effect. The strategy given here is an effective route to the SERS-based detection of the soluble molecules, which are of small Raman scattering cross-section and hardly adsorbed on the SERS substrates, by choosing proper solvents, but not suitable for the volatile soluble molecules as the liquid film cannot confine these molecules.

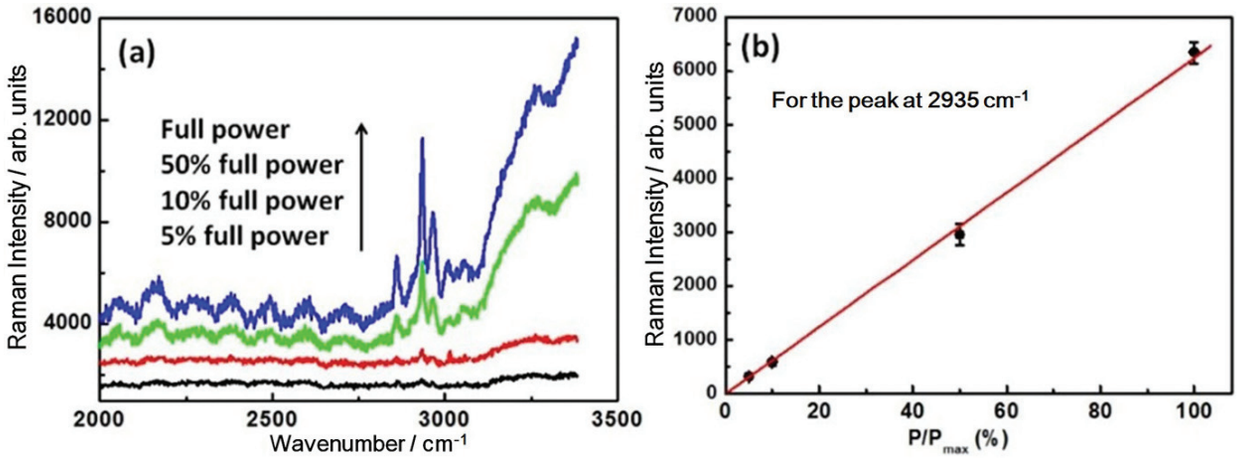

Figure 7. (a) The Raman spectra of DMMP aqueous solution droplet on the substrate, under the excitation with different laser powers (P), after the evaporation for the same duration. The maximal excitation power of the equipment P_{max} = 17 mW. (b) The plot of the intensity of the peak at 2936 cm^{-1} versus the laser excitation power [the data are from (a)]. The solid line is the linear fitting results [33].

3. The surface modification and amidation reaction

In addition to the abovementioned thin water film confinement strategy, here, we introduce another approach to the SERS-based ultrasensitive detection of metal weakly interacted organophosphorus nerve agent sarin based on surface modification of the SERS substrates and amidation reaction [42]. The methanephosphonic acid (MPA) was chosen as the sarin simulation agent (or the target molecule). The Au-coated Si nanocone array was surface-modified with 2-aminoethanethiol molecules and used as the SERS-substrate for detection of MPA. It has been demonstrated that the modified substrate can selectively capture MPA in the solution under the existence of the coupling agent, and hence realize the SERS-based detection of the MPA in the solution with good selectivity and high sensitivity.

3.1. Surface modification-based SERS detection strategy

3.1.1. Choice of sarin-simulated agent

For convenient study of SERS-based detection of sarin, its simulation agent should be chosen. Such simulation agent should be of less or moderate toxicity but the chemical properties and especially the Raman spectrum should be similar to sarin. It has been found that methanephosphonic acid (MPA) is also a suitable simulation agent for sarin, in addition to the commonly used DMMP. The molecular formula of sarin and MPA are $(CH_3)_2CHOOPF(CH_3)$ and CH_5O_3P, respectively. Both have the C-P bonds and the similar bond length, chemically belonging to the organophosphorus group. Both MPA and sarin can produce amidation reaction with amino compounds [43]. It is expected that these similarities in chemical structures could have similar Raman spectral pattern to each other.

The Raman spectra of sarin and MPA were simulated based on density functional theory (DFT) by means of the Gaussian 09 software [44]. **Figure 8(a)** is the measured Raman spectrum for the pure MPA. The simulated Raman spectrum is very similar in the primary and minor peaks except the small difference in the peak positions, demonstrating the validity of the spectral simulations. **Figure 8(b)** shows the simulated Raman spectrum of sarin. Correspondingly, the

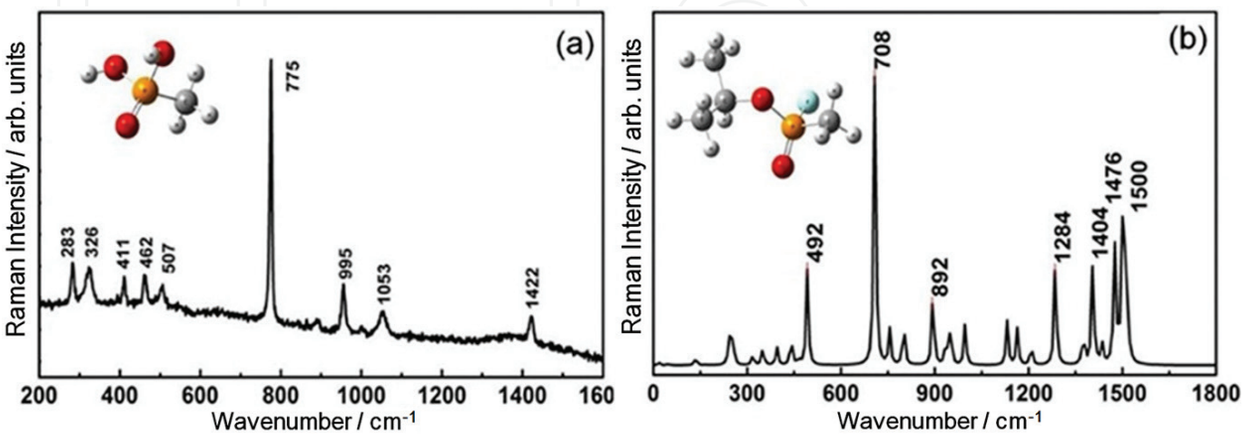

Figure 8. The Raman spectra for MPA (a) and sarin (b). (a) The measured Raman spectrum of pure MPA (excited by 785 nm laser). (b) The simulated Raman spectrum of sarin based on DFT calculations [42].

vibrational peaks can be assigned according to the DFT calculations [42]. The Raman spectral bands are mostly similar in wavenumbers for sarin and MPA. The MPA can thus be used as a sarin-simulated agent.

3.1.2. Surface modification of SERS substrate

Generally, the Raman signals could be detected only when the MPA molecules are adsorbed on the SERS substrates. However, the MPA molecules can hardly be adsorbed on the noble metals, due to the weak interaction between them. The surface modification strategy was used to overcome such problem. A surface modifier should be chosen in such a way that it can strongly interact with both the SERS substrate and MPA molecules.

The 2-aminoethanethiol molecule contains two-head groups such as amino and thiol groups. It is well known that there is a strong covalent bond interaction between thiol and gold according to the theory of hard and soft (Lewis) acids and bases [45, 46]. As for the amino group, it can react with phosphonic group to generate phsophonamidate in the presence of coupling agents [such as dicyclohexylcarbodiimide, N, N-diisopropylcarbodiimide, 1-ethyl-3-(3-(dimethylamino) propyl) carbodimide] [47]. Therefore, the thiol groups in 2-aminoethanethiol molecules would tend to be bound with gold substrate to form Au—S covalent bonds, and the amino groups would selectively capture phosphonic groups in MPA molecules in the solution, as schematically shown in **Figure 9**. 2-Aminoethanethiol could thus be a suitable modifying agent of the SERS substrate. It is expected that the surface-modified SERS substrate would selectively capture the organophosphorus molecules (such as sarin, MPA), as demonstrated in **Figure 9**. In this case, we could realize detection of MPA or sarin based on the SERS effect.

3.2. SERS measurements

3.2.1. Surface-modified SERS substrate

Au-coated Si nanocone array was used as the SERS substrate, which was prepared by sputtering deposition of gold on the Si nanocone array induced by PS colloidal monolayer and plasma etching strategy, as previously described in detail [42]. **Figure 10** shows the Si nanocone array before and after sputtering deposition with a gold layer about 10 nm in thickness. Such array is of good uniformity in structure.

Such Au-coated Si nanocone array was immersed into the ethanol solution of 2-aminoethanethiol (1 mM) for surface modification. FTIR spectral measurement has confirmed that the modified

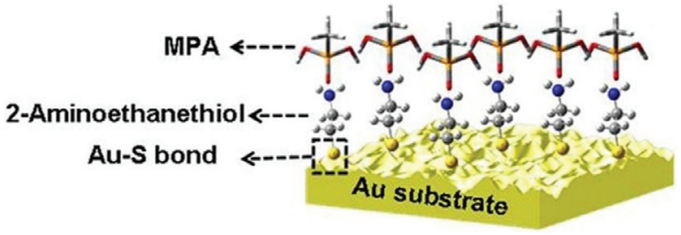

Figure 9. Schematic illustration for the interaction of the modifying agent (2-aminoethanethiol) with MPA molecules and SERS substrate (gold) [42].

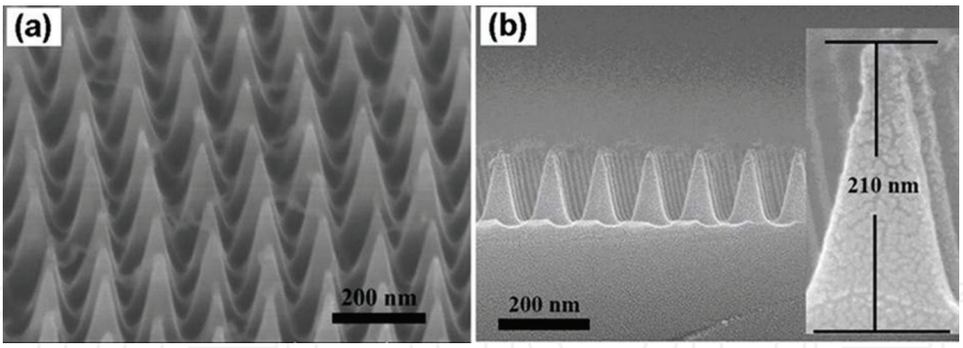

Figure 10. The morphology of the as-prepared nanocone array. (a) The FESEM image of the Si nanocone array induced by plasma etching the PS colloidal monolayer on Si wafer. (b) The cross sectional image after sputtering deposition of gold on the Si nanocone array. The inset: A magnified image of a single Au-coated cone [42].

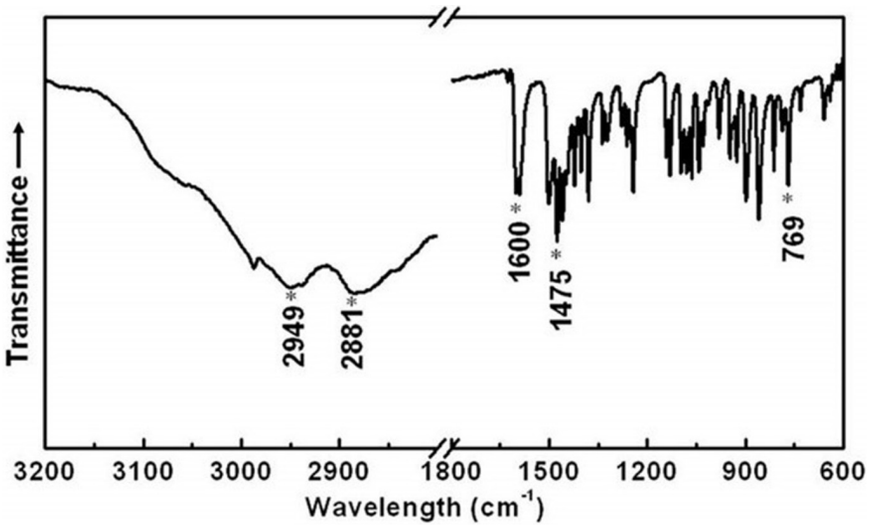

Figure 11. FTIR spectrum of the surface-modified au-coated Si cone array [42].

2-aminoethanethiol molecules were bound with the Au film on the array's surface by the thiol group, as shown in **Figure 11**. The peaks at 2881 and 2949 cm^{-1} are attributed to the symmetry stretching and asymmetry vibration of the CH_2 in 2-aminoethanethiol [48], while the peak at 1600 cm^{-1} is ascribed to the in-plane bending vibration of the NH_2 groups in 2-aminoethanethiol [48]. In addition, the peak at 1475 cm^{-1} originates from the shear vibration of the CH_2 in 2-aminoethanethiol [48]. Furthermore, the peak at 769 cm^{-1} is assigned to swing plane vibration of CH_2 chains, corresponding to the two methylene groups in 2-aminoethanethiol molecules [48]. It could thus be concluded that the modified array's surface was rich of 2-aminoethanethiol molecules.

3.2.2. Raman spectral measurements

The modified substrate was then immersed into the ethanol solution of MPA in the presence of the coupling agent 1-ethyl-3-(3-(dimethylamino) propyl) carbodimide (or EDC for short) (2 mM) for 3 h which was long enough to reach the equilibrium adsorption of the MPA on

the SERS substrate. Here, the coupling agent EDC was employed to activate phosphonic groups in MPA molecules for coupling with the primary amines in the modifying agent. Finally, the soaked substrate was taken out and cleaned with deionized water and ethanol to remove any unbound molecules, and dried in the flow of N_2 prior to the SERS spectral measurement under excitation at 785 nm and exposure time 10 s.

The Raman spectral pattern. Figure 12 demonstrates the Raman spectrum of the surface-modified Au-coated Si nanocone array after immersion in the MPA solution (10^{-3} M) with EDC. The Raman peaks at 643, 725, 976, 1025, 1212, 1412, and 1445 cm^{-1} are clearly observed, as shown in curve (I) of **Figure 12**. On the contrary, for the surface-modified array without immersion or after immersion in the EDC solution without MPA or in the MPA solution without EDC, no Raman peak was detected, as illustrated in curves (II, III, IV) of **Figure 12**. So the Raman peaks in curve (I) of **Figure 12** should be associated with the coexistence of MPA and EDC. By comparing with **Figure 8(a)**, however, we can know that the Raman spectrum in curve (I) is completely different from that of the pure MPA. It means that the Raman peaks in **Figure 12** are not attributed to MPA directly.

Concentration dependence. Further, the concentration-dependent Raman spectra were measured for the surface-modified SERS substrate (or Au-coated Si nanocone array) after soaking in the MPA solutions with different concentrations in the presence of EDC, as shown in **Figure 13(a)**. The intensities of all Raman peaks increase with the rising MPA concentration in the solutions. The peak intensity I is approximately subject to the linear double logarithmic relation with the MPA concentration $\boldsymbol{C}$ from 10^{-8} to 10^{-2} M (or ~1 to ~1000 ppm), or

$$LogI = A_0 + B_0 \cdot LogC \tag{12}$$

where $\boldsymbol{A_o}$ and $\boldsymbol{B_0}$ are the constants independent of the concentration. **Figure 13(b)** shows the typical result corresponding to the main peak at 976 cm^{-1}, exhibiting a good linear relation.

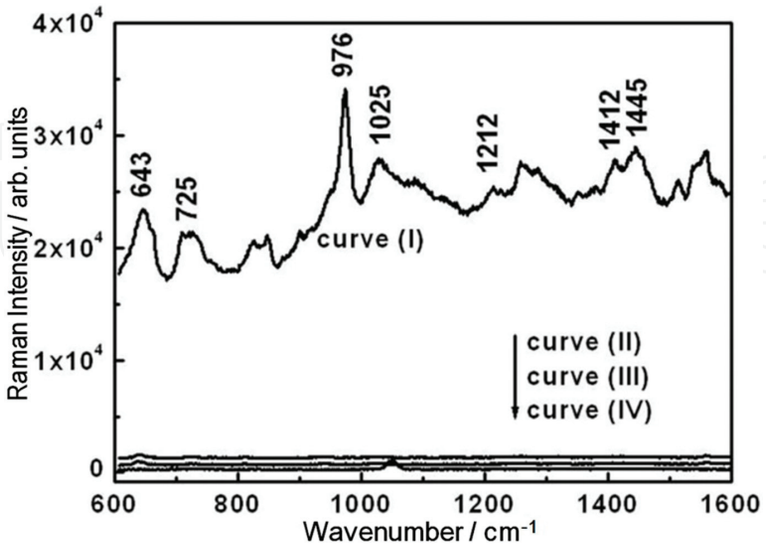

Figure 12. The Raman spectra for the Au-coated Si nanocone array after soaking in different solutions for 3 h. Curve (I): After soaking in the MPA solution (10^{-3} M) with the EDC. Curve (II): The array without immersion; curve (III): After soaking in the EDC solution without MPA; curve (IV): After soaking in the MPA solution without EDC [42].

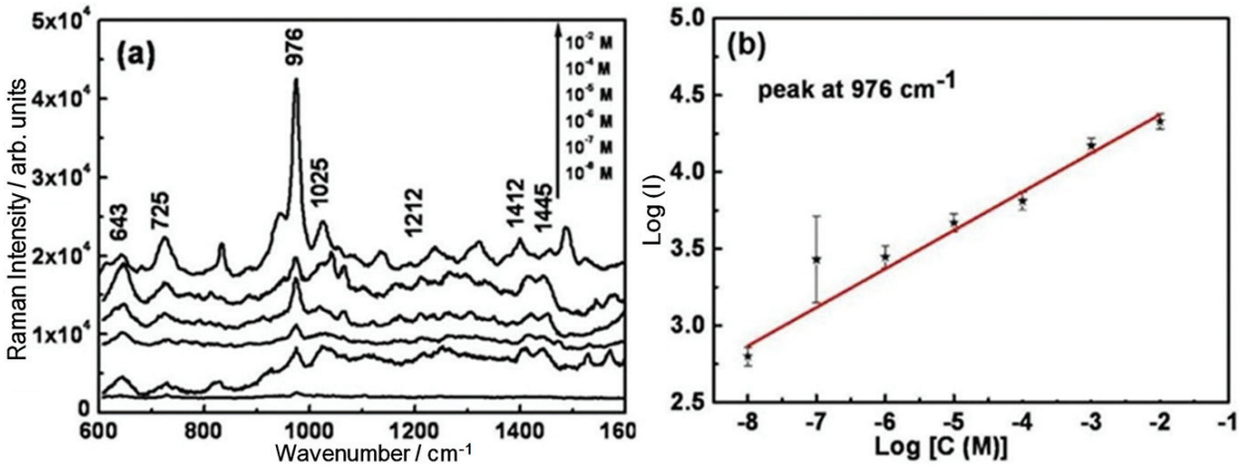

Figure 13. (a) The Raman spectra for the surface-modified Au-coated Si nanocone array after soaking in the MPA solutions with different concentrations in the presence of EDC. (b) Plot of the logarithmic peak intensity (***I***) at 976 cm^{-1} versus the logarithmic MPA concentration (***C***) [the data are from (a)]. The straight line is the linear fitting results [42].

The parameter B_0 value is about 0.25 by fitting. We can thus rewrite Eq. (12) as a power function, or

$$I = M \cdot C^{0.25} \tag{13}$$

where ***M*** is the constant independent of the concentration ***C***.

3.3. Amidation reaction

Regarding the Raman spectral origin and their evolution, it can be attributed to adsorption of MPA molecules and subsequent amidation reaction on the SERS substrate's surface, as schematically illustrated in **Figure 14**.

3.3.1. Amidation reaction-induced Raman spectra

After the coupling agent EDC was added to the ethanol solution of MPA, the coupling between them would activate the phosphonic groups in MPA [see **Figure 14(a)**] [47]. When the surface-modified SERS substrate was subsequently immersed into the MPA solution, because of the strong interaction between the amino groups in 2-aminoethanethiol and the phosphonic groups in the activated MPA molecules [47], the activated MPA molecules would diffuse onto and be adsorbed on the substrate's surface, as illustrated in **Figure 14(b)**.

At this time, the adsorbed MPA molecules could react with the 2-aminoethanethiol molecules on the Au-coated Si cone array due to the amino groups in the 2-aminoethanethiol [47], or the amidation reaction between them

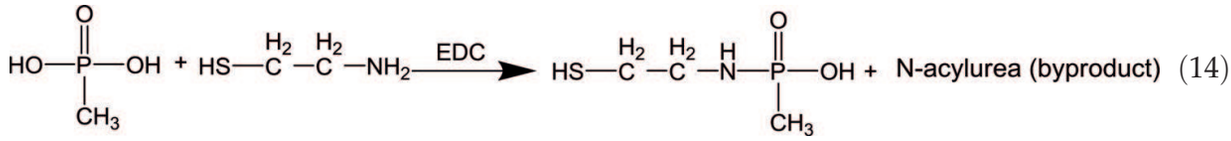

(14)

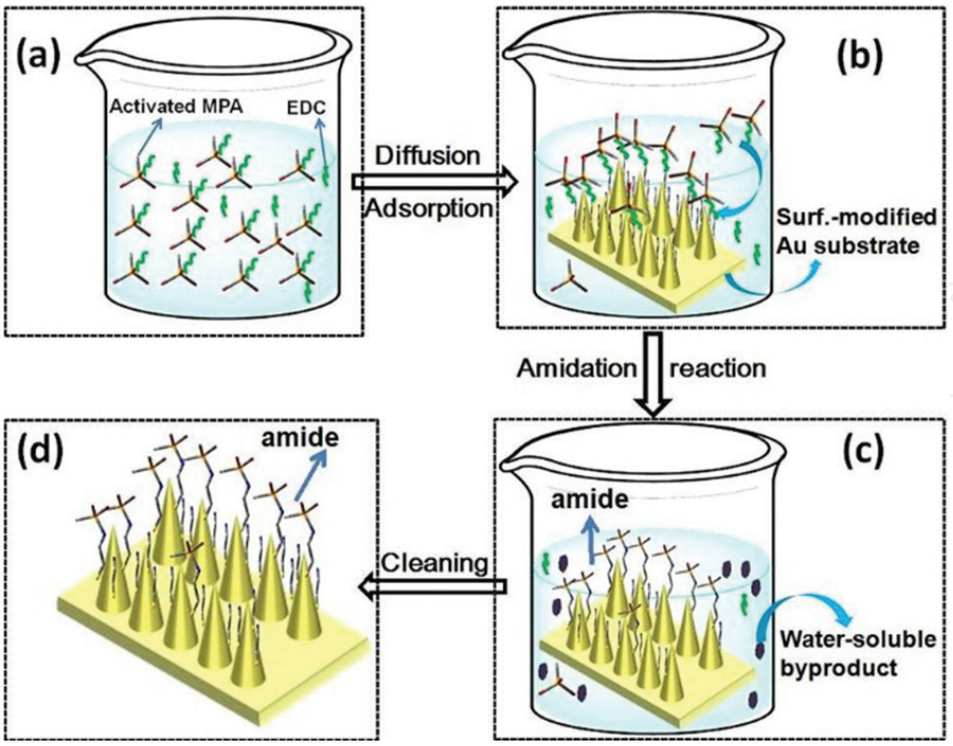

Figure 14. The schematic illustration for the MPA molecules' adsorption and amidation reaction on the Au-coated Si nanocone array. (a) Ethanol solution of the EDC-activated MPA. (b) The activated MPA molecules diffuse into and are adsorbed on the surface-modified array. (c) The amidation reaction on the substrate is finished. (d) The reaction products (organic phosphorus amide molecules) are bound to the substrate [42].

would occur on the surface of the array. The reaction products N-(2-mercaptoethyl)-P-methylphosphonamidic acid $C_3H_{10}O_2NPS$ should be formed and bound or anchor on the surface of the array [see **Figure 14(c)**]. Besides, the byproduct N-acylurea was also produced in the solution. It is water-soluble and removable before Raman spectral measurement [see **Figure 14(d)**]. So, the Raman spectrum shown in curve (I) of **Figure 12** could be ascribed to the product $C_3H_{10}O_2NPS$ on the substrate.

Evidently, the higher MPA content in the solution would induce the more activated MPA molecules adsorbed on the modified Au-coated Si nanocone array, and the more reaction products $C_3H_{10}O_2NPS$ bound on the array. This would result in higher Raman peak intensity, showing increase of the Raman peak intensity with the rising MPA content in the solutions, as illustrated in **Figure 13(a)**.

Quantitatively, as mentioned earlier, the concentration-dependent Raman intensity can be described by a power function [see Eq. (13)]. It should be associated with the adsorption behavior of the MPA molecules on the modified substrate. According to the Freundlich theory [49], the adsorption of molecules on a heterogeneous surface could be described by:

$$q_e = K_F \cdot C^{\frac{1}{n}} \tag{15}$$

where q_e is the equilibrium adsorption amount, the parameters K_F and n are the parameters reflecting the adsorption capacity and adsorption intensity, respectively. Obviously, the

intensity ***I*** of a Raman peak should be proportional to the number density of the molecules adsorbed on the substrate within the area of a laser spot or show a linear relation with the adsorption amount ***q***:

$$I = K_0 \cdot q \tag{16}$$

where $\boldsymbol{K_0}$ is the constant. By combining Eqs. (15) and (16), we have the relationship between the intensity of Raman signal and the MPA concentration in the soaking solution:

$$I = K \cdot C^{\frac{1}{n}} \tag{17}$$

where $K = K_0 \cdot K_F$. Eq. (17) is in complete agreement with Eq. (13), which has also confirmed the Freundlich-typed adsorption of the MPA molecules on the substrate. By combining Eqs. (13) and (17), the value of MPA adsorption parameter (***n***) can thus be estimated to be $\boldsymbol{n} = 4$. This also presents a simple way to measure the adsorption parameters, which are normally acquired by the time-consuming measurement of the adsorption isotherms.

3.3.2. Confirmation of the amidation reaction

For confirmation of reaction (9) occurring on surface of the substrate, the amidation reaction experiment was carried out, according to Vijay et al.'s method [50], by preparing the ethanol solution with EDC, MPA and 2-aminoethanethiol and continuously stirring it at room temperature for 15 h, as previously described in detail [42]. The pure amidation compound was thus acquired. The FTIR measurement was conducted for this compound, as shown in **Figure 15**. All peaks can be ascribed to the vibrations of N-(2-mercaptoethyl)-P-methylphosphonamidic acid ($C_3H_{10}O_2NPS$) [51]. For instance, the peaks at 731, 768 and 812 cm^{-1}correspond to twisting vibrations of the carbon chains $(CH_2)_2$ in $C_3H_{10}O_2NPS$; the peak at 894 cm^{-1} is assigned to the stretching vibration of (P—CH_3) + (P—O); and the peaks at 1041 and 1064 cm^{-1} are from the stretching vibrations of (C—N) [48]. These indicated that pure amide $C_3H_{10}O_2NPS$ was obtained.

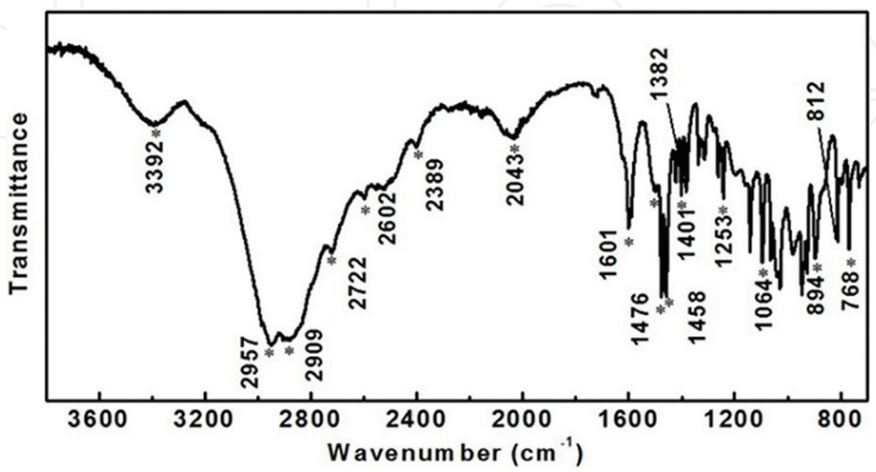

Figure 15. FTIR spectrum of the products after amidation reaction [42].

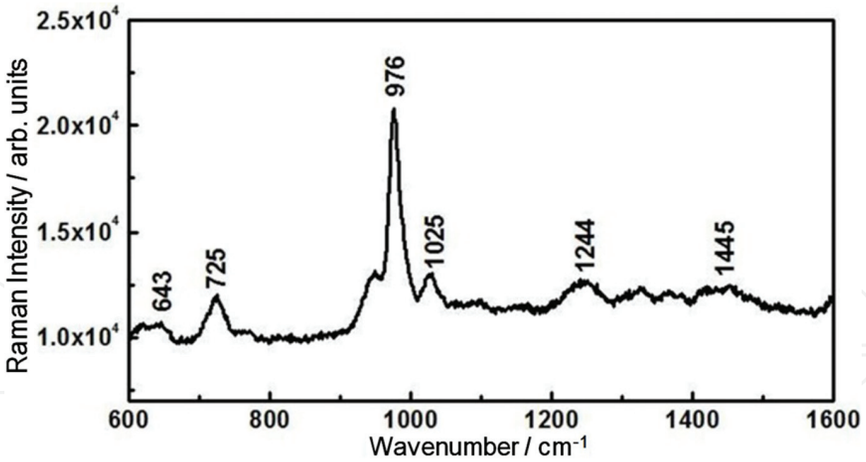

Figure 16. The Raman spectrum for the Au-coated Si nanocone array after immersion in the ethanol solution with 1.0×10^{-3} M $C_3H_{10}O_2NPS$ [42].

For the Raman spectral measurements, the pure amide ($C_3H_{10}O_2NPS$) was diluted, with ethanol, to a given concentration. The Au-coated Si nanocone array was then immersed into the $C_3H_{10}O_2$-NPS-contained ethanol solution before the Raman spectral measurements. **Figure 16** shows the results corresponding to the solution with 1.0×10^{-3} M in $C_3H_{10}O_2NPS$ concentration. The spectral pattern is in good agreement with that shown in curve (I) of **Figure 12**. So, the Raman spectrum in curve (I) of **Figure 12** should be attributed to the amidation compound $C_3H_{10}O_2NPS$. These results have confirmed that the amidation reaction occurred on the surface of the modified Au-coated Si nanocone array during its immersion in the MPA solutions with EDC, and that the reaction products $C_3H_{10}O_2NPS$ molecules were formed on and bound with the array's surface.

3.4. Quantitative SERS-based detection of MPA

As mentioned earlier, the Au-coated Si nanocone array modified with 2-aminoethanethiol can capture selectively MPA in the solution in the presence of EDC via diffusion and adsorption, leading to the amidation reaction and the formation of $C_3H_{10}O_2NPS$ molecules which were still bound on the array's surface. The bound $C_3H_{10}O_2NPS$ molecules were corresponding to the MPA molecules adsorbed on the SERS substrate. Therefore, by using the 2-aminoethanethiol-modified Au-coated Si nanocone array, we can realize the SERS-based ultrasensitive and quantitative detection of MPA in the solution. The obtained Raman spectra are from the $C_3H_{10}O_2NPS$ molecules but corresponding to the MPA, which exhibits a linear double logarithmic relation between the Raman peak intensity and the MPA concentration, as described in Eq. (4). Since there exist similarities between MPA and sarin in chemical properties and Raman spectral pattern, as mentioned in Section 3.1.1, it is thus expected that the abovementioned method is also suitable for sarin detection.

Finally, it should be mentioned that the method introduced here relies on the activation of phosphonic groups by the coupling agent EDC which creates reactive phosphonamide. Both EDC and the by-product N-acylurea can be removed by subsequent substrate cleaning before Raman spectral measurement.

4. Conclusions and outlook

We have introduced some recent progresses in the SERS-based detection of the organophosphorus nerve agents, including the thin water film confinement evaporation concentrating strategy and the SERS substrates' surface modification/amidation reaction. For the former, when the solution containing target molecules is dropped on the SERS substrate and forms a thin water film on it, the target molecules are limited within the film. Subsequent water evaporation leads to the enrichment or concentrating of the target molecules within the region of strongly enhanced electromagnetic field above the substrate, and hence significantly enhances the Raman signal or induces the CERS effect. The validity of this strategy has been demonstrated by taking the sarin simulant DMMP as the target molecule, which are hardly adsorbed on the gold substrates, exhibiting significant CERS effect during water film evaporation and showing a good linear relation between the reciprocal intensity for the Raman characteristic peak and the evaporation interval, which is in agreement with quantitative description of evaporation-induced solute concentrating. The thin water film not only confines the target molecules within a limited space but also protects the target molecules from laser-induced damage. This approach should also be suitable for the other soluble molecules with low volatility. For the latter, because the 2-aminoethanethiol molecules possess two-head groups: amino and thiol groups: one can be bound with gold film and the other can capture the phosphonic groups in sarin simulation agent MPA in presence of the coupling agent EDC, the 2-aminoethanethiol-modified SERS substrate could selectively capture MPA molecules in the solution, which thus induces the amidation reaction on the substrate's surface. The reaction products or $C_3H_{10}O_2NPS$ molecules are still bound on the substrate's surface. Correspondingly, we could obtain the Raman spectra of amide $C_3H_{10}O_2NPS$, which correspond to the MPA molecules adsorbed on the substrate. The Raman peak intensity shows a good linear double logarithmic relation with the MPA concentration in a large range, which could be attributed to Freundlich adsorption behavior of MPA on the surface-modified SERS substrate. The minimum detection level of MPA is down to ~1 ppb. We can thus quantitatively detect MPA or sarin in solutions based on the SERS effect. This route could also be suitable for the other organophosphorus nerve agents and some other molecules weakly interacted with the coin metal substrates by choosing appropriate modifiers. In a word, the abovementioned progresses provide new ways for highly efficient SERS-based detection of the organophosphorus nerve agents and some other target molecules that weakly interact with the coin metal substrates.

Acknowledgements

This work is financially supported by the National Key Research and Development Program of China《Fundamental Research on nano sensing materials and high performance sensors focused on pollutants detection》(Grant No. 2017YFA0207101), Natural Science Foundation of China (Grant No. 51531006, 11574313, 11374300 and 51571188) and the CAS/SAF International Partnership Program for Creative Research Teams.

Author details

Qian Zhao, Guangqiang Liu* and Weiping Cai*

*Address all correspondence to: liugq@issp.ac.cn and wpcai@issp.ac.cn

Key Lab of Materials Physics, Anhui Key Lab of Nanomaterials and Nanotechnology, Institute of Solid State Physics, Chinese Academy of Sciences, Hefei, PR China

References

[1] Federation of American Scientists. Types of Chemical Weapons [Internet]. 2015. Available from: https://fas.org/cw/documents/cwagents.pdf

[2] Yang YM, Ji HF, Thundat T. Nerve agents detection using a Cu^{2+}/L-cysteine bilayer-coated microcantilever. Journal of the American Chemical Society. 2003;**125**:1124-1125. DOI: 10.1021/ja028181n

[3] Guilbault GG, Kristoff J. Detection of organophosphorus compounds with a coated piezoelectric crystal. Analytical Chemistry. 1985;**57**:1754-1756. DOI: 10.1021/ac00285a057

[4] Riter LS, Peng YN, Noll RJX. Analytical performance of a miniature cylindrical ion trap mass spectrometer. Analytical Chemistry. 2002;**74**:6154-6162. DOI: 10.1021/ac0204956

[5] Steiner WE, Klopsch SJ, English WA. Detection of a chemical warfare agent simulant in various aerosol matrixes by ion mobility time-of-flight mass spectrometry. Analytical Chemistry. 2005;**77**:4792-4799. DOI: 10.1021/ac050278f

[6] Fleischmann M, Hendra PJ, McQuilla AJ. Raman spectra of pyridzne adsorbed at a silver electrode. Chemical Physics Letters. 1974;**26**:163-166. DOI: 10.1016/0009-2614(74)85388-1

[7] Albrecht MG, Creighton JA. Anomalously intense Raman spectra of pyridine at a silver electrode. Journal of the American Chemical Society. 1977;**99**:5215-5217. DOI: 10.1021/ja00457a071

[8] Jeanmaire DL, Vanduyne RP. Surface Raman spectroelectrochemistry: Part I. Heterocyclic, aromatic, and aliphatic amines adsorbed on the anodized silver electrode. Journal of Electroanalytical Chemistry. 1977;**84**:1-20. DOI: 10.1016/S0022-0728(77)80224-6

[9] Lin EC, Fang J, Park SCX. Effective localized collection and identification of airborne species through electrodynamic precipitation and SERS-based detection. Nature Communications. 2013;**4**:1-8. DOI: 10.1038/ncomms2590

[10] Cecchini MP, Turek VA, Paget JX. Self-assembled nanoparticle arrays for multiphase trace analyte detection. Nature Materials. 2013;**12**:165-171. DOI: 10.1038/nmat3488

[11] Lim DK, Jeon KS, Hwang JH. Highly uniform and reproducible surface-enhanced Raman scattering from DNA-tailorable nanoparticles with 1-nm interior gap. Nature Nanotechnology. 2011;**6**:452-460. DOI: 10.1038/nnano.2011.79

[12] Wang YQ, Yan B, Chen LX. SERS tags: Novel optical nanoprobes for bioanalysis. Chemical Reviews. 2013;**113**:1391-1428. DOI: 10.1021/cr300120g

[13] Alvarez-Puebla RA, Liz-Marzan LM. Traps and cages for universal SERS detection. Chemical Society Reviews. 2012;**41**:43-51. DOI: 10.1039/C1CS15155J

[14] Wu DY, Li JF, Ren BX. Electrochemical surface-enhanced Raman spectroscopy of nanostructures. Chemical Society Reviews. 2008;**37**:1025-1041. DOI: 10.1039/B707872M

[15] Tao A, Kim F, Hess CX. Langmuir–Blodgett silver nanowire monolayers for molecular sensing using surface-enhanced Raman spectroscopy. Nano Letters. 2003;**3**:1229-1233. DOI: 10.1021/nl0344209

[16] Xiong YJ, McLellan JM, Chen JY. Kinetically controlled synthesis of triangular and hexagonal nanoplates of palladium and their SPR/SERS properties. Journal of the American Chemical Society. 2005;**127**:17118-17127. DOI: 10.1021/ja056498s

[17] Li JF, Huang YF, Ding YX. Shell-isolated nanoparticle-enhanced Raman spectroscopy. Nature. 2010;**464**:392-395. DOI: 10.1038/nature08907

[18] Stuart DA, Biggs KB, Van-Duyne RP. Surface-enhanced Raman spectroscopy of half-mustard agent. The Analyst. 2006;**131**:568-572. DOI: 10.1039/B513326B

[19] Habouti S, Mátéfi-Tempfli M, Solterbeck CH. On-substrate, self-standing au-nanorod arrays showing morphology controlled properties. Nano Today. 2011;**6**:12-19. DOI: 10.1016/j.nantod.2010.11.001

[20] Moskovits M. Surface-enhanced Raman spectroscopy: A brief retrospective. Journal of Raman Specroscopy. 2005;**36**:485-496. DOI: 10.1002/jrs.1362

[21] SSR D, Singh AK, Senapati DX. Gold nanoparticle based label-free SERS probe for ultrasensitive and selective detection of trinitrotoluene. Journal of the American Chemical Society. 2009;**131**:13806-13812. DOI: 10.1021/ja905134d

[22] Camden JP, Dieringer JA, Wang YM. Probing the structure of single-molecule surface-enhanced Raman scattering hot spots. Journal of the American Chemical Society. 2008;**130**:12616-12617. DOI: 10.1021/ja8051427

[23] Huang Y, Dai L, Song L. Engineering gold nanoparticles in compass shape with broadly tunable plasmon resonances and high-performance SERS. ACS Applied Materials & Interfaces. 2016;**8**:27949-27955. DOI: 10.1021/acsami.6b05258

[24] Sajanlal PR, Pradeep T. Functional hybrid nickel nanostructures as recyclable SERS substrates: Detection of explosives and biowarfare agents. Nanoscale. 2012;**4**:3427-3437. DOI: 10.1039/C2NR30557G

[25] Tang HB, Meng GW, Huang QX. Arrays of cone-shaped ZnO nanorods decorated with Ag nanoparticles as 3D surface-enhanced Raman scattering substrates for rapid detection of trace polychlorinated biphenyls. Advanced Functional Materials. 2012;**22**:218-224. DOI: 10.1002/adfm.201102274

[26] Dieringer JA, RB L-II, Scheidt KA. A frequency domain existence proof of single-molecule surface-enhanced Raman spectroscopy. Journal of the American Chemical Society. 2007;**129**:16249-16256. DOI: 10.1021/ja077243c

[27] Bell SEJ, Sirimuthu NMS. Surface-enhanced Raman spectroscopy (SERS) for sub-micromolar detection of DNA/RNA mononucleotides. J. Am. Chem. Soc. 2006;**128**: 15580-15581. DOI: 10.1021/ja066263w

[28] Nie S, Emory SR. Probing single molecules and single nanoparticles by surface-enhanced Raman scattering. Science. 1997;**275**:1102-1106. DOI: 10.1126/science.275.5303.1102

[29] Kneipp K, Wang Y, Kneipp HX. Single molecule detection using surface-enhanced Raman scattering (SERS). Physical Review Letters. 1997;**78**:1667-1670. DOI: 10.1103/PhysRevLett.78.1667

[30] Moskovits M. Surface-enhanced spectroscopy. Rev. Mod. Phys. 1985;**57**:783-826. DOI: 10.1103/RevModPhys.57.783

[31] Lee SJ, Morrill AR, Moskovits M. Hot spots in silver nanowire bundles for surface-enhanced Raman spectroscopy. Journal of the American Chemical Society. 2006;**128**: 2200-2201. DOI: 10.1021/ja0578350

[32] Sharma B, Frontiera RR, Henry AI. SERS: Materials, applications, and the future. Materials Today. 2012;**15**:16-25. DOI: 10.1016/S1369-7021(12)70017-2

[33] Wang JJ, Duan GT, Liu G. Detection of dimethyl methylphosphonate by thin water film confined surface-enhanced Raman scattering method. Journal of Hazardous Materials. 2016;**303**:94-100. DOI: 10.1016/j.jhazmat.2015.10.022

[34] Taranenko N, Alarie JP, Stokes DL. Surface-enhanced Raman detection of nerve agent simulant (DMMP and DIMP) vapor on electrochemically prepared silver oxide substrates. Journal of Raman Specroscopy. 1996;**27**:379-384. DOI: 10.1002/(SICI)1097-4555(199605)27:5<379::AID-JRS925>3.0.CO;2-G

[35] Pearman WF, Fountain AW. Classification of chemical and biological warfare agent simulants by surface-enhanced Raman spectroscopy and multivariate statistical techniques. Applied Spectroscopy. 2006;**60**:356-365. DOI: 10.1366/000370206776593744

[36] Yan F, Tuan VD. Surface-enhanced Raman scattering detection of chemical and biological agents using a portable Raman integrated tunable sensor. Sensors and Actuators B: Chemical. 2007;**121**:61-66. DOI: 10.1016/j.snb.2006.09.032

[37] Kim NJ. Physical origins of chemical enhancement of surface-enhanced Raman spectroscopy on a gold nanoparticle-coated polymer. Journal of Physical Chemistry C. 2010;**114**:13979-13984. DOI: 10.1021/jp103360m

[38] Wang JJ, Duan GT, Liu G. Gold quasi rod-shaped nanoparticle-built hierarchically micro/nanostructured pore array via clean electrodeposition on a colloidal monolayer and its structurally enhanced SERS performance. Journal of Materials Chemistry. 2011;**21**:8816-8821. DOI: 10.1039/C1JM10773A

[39] Van-der-Veken B, Herman M. Vibrational spectra of $CH_3PO(OCH3)_2$ and isotopically substituted derivatives. Phosphorus. Sulfur. 1981;**10**:357-367. DOI: 10.1080/03086648108077388

[40] Christesen SD. Raman cross sections of chemical agents and simulants. Applied Spectroscopy. 1988;**42**:318-321. DOI: 10.1366/0003702884428220

[41] Tomchenko AA, Harmer GP, Marquis BT. Detection of chemical warfare agents using nanostructured metal oxide sensors. Sensors and Actuators B: Chemical. 2005;**108**:41-45. DOI: 10.1016/j.snb.2004.11.059

[42] Zhao Q, Liu GQ, Zhang HW. SERS-based ultrasensitive detection of organophosphorus nerve via substrate's surface modification agents. Journal of Hazardous Materials. 2017;**324**:194-202. DOI: 10.1016/j.jhazmat.2016.10.049

[43] Montalbetti CAGN, Falque V. Amide bond formation and peptide coupling. Tetrahedron. 2005;**61**:10827-10852. DOI: 10.1016/j.tet.2005.08.031

[44] Costa JCS, Ando RA, Sant'Ana AC. Surface-enhanced Raman spectroscopy studies of organophosphorous model molecules and pesticides. Physical Chemistry Chemical Physics. 2012;**14**:15645-15651. DOI: 10.1039/C2CP42496G

[45] Pearson RG. Hard and soft acids and bases, HSAB, part 1: Fundamental principles. Journal of Chemical Education. 1968;**45**:581-587

[46] Pearson RG. Hard and soft acids and bases, HSAB, part II: Underlying theories. Journal of Chemical Education. 1968;**45**:643-648

[47] Raghav R, Srivastava S. Immobilization strategy for enhancing sensitivity of immunosensors: L-asparagine-AuNPs as a promising alternative of EDC-NHS activated citrate-AuNPs for antibody immobilization. Biosensors & Bioelectronics. 2016;**78**:396-403. DOI: 10.1016/j.bios.2015.11.066

[48] Speight JG. Section 3(3.1) Infrared absorption spectroscopy. In: Speight JG, editor. Lange's Handbook of Chemistry. 16th ed. Wyoming: The McGraw-Hill Companies Inc.; 2005. pp. 3.3-3.36

[49] Freundlich H, Heller W. The adsorption of cis- and trans-azobenzene. Journal of the American Chemical Society. 1939;**61**:2228-2230

[50] Sehgal D, Vijay IK. A method for the high-efficiency of water-soluble carbodiimide-mediated amidation. Analytical Biochemistry. 1994;**218**:87-91. DOI: 10.1006/abio.1994.1144

[51] Speight JG. Section 3(3.1) Infrared absorption spectroscopy. In: Speight JG, editor. Lange's Handbook of Chemistry. 16th ed. Wyoming: The McGraw-Hill Companies Inc; 2005. pp. 3.3-3.23

IntechOpen